ADVANCED ENGINEERING MATERIALS
www.aem-journal.com

Modeling the Solvolysis of Composite Materials of Wind Turbine Blades

Yi Chen and Leon Mishnaevsky Jr.*

A computational model of the depolymerization of composites during solvolysis of wind turbine blades is developed. The model is based on a phenomenological approach, describing the dissolution of an epoxy matrix as a local phase transition influenced by temperature, solvent diffusion, and local microstructures. The model is implemented in the finite element code Abaqus, using the user-defined field and heat flux subroutines. Parametric studies are carried out to study the influence of defects and heterogeneities on the depolymerization of composite materials. The results show that variations of the solvent diffusivity in the vicinity of fiber/matrix lead to nonhomogeneity of depolymerization, and smaller diffusivity may explain matrix residues remaining on the fibers. Fiber volume density and distribution influence the polymer dissolution rate because the resistance to solvent diffusion arises between fibers. Further, voids in the polymer may lead to a local acceleration of the polymer dissolution. This work also looks into the contributions of diffusion and reaction to depolymerization, and the former dominates. The rate and homogeneity of depolymerization, therefore, depend significantly on the manufacturing quality of composites.

1. Introduction

Over the following decades, a large expansion of wind energy generation in Europe is foreseen. The goal is to cover 30% of the European Union's electricity demand with wind energy by 2030.[1] At the same time, the wind turbines installed during the 2000s are approaching the end of their planned lifetime. While many parts of wind turbines can be well recycled, this is different for composite blades, which have been designed to sustain extreme mechanical and environmental loads for decades. Across Europe, more than 70 000 wind turbines are spinning with a combined capacity of 189 gigawatts, while a single megawatt of installed capacity can lead to dozens of tons of composite waste.[2,3] 14 000 wind turbine blades need to be recycled by 2023.[4] Additionally, more blades are on the way for recycling, as almost 52 000 tons of blades are expected to be decommissioned every year by 2030.[5]

A typical wind turbine blade consists of glass/carbon fibers, thermosets (such as epoxy and polyester), thermoplastics (such as polyvinyl chloride), wood, adhesives, and coatings.[6] Various strategies are available for the end-of-life management of wind turbine blades, including reuse, refurbishment, and recycling.[7] Recycling is a less preferable option compared to waste reduction, recovery, and repair. However, under numerous circumstances, recycling becomes the most viable and necessary step: it is impractical to repurpose all 52 000 tons of blades annually for applications such as bus stops or bridges; not all structures can be perpetually repaired, and certain waste generation is inevitable. Among the existing recycling methods (mechanical shredding, crushing, pyrolysis, solvolysis, etc.), chemical recycling, particularly solvolysis, is relatively controllable and yields relatively clean fibers, necessitating lower temperatures than pyrolysis.[8]

During the solvolysis of composites, the polymer matrix undergoes chemical decomposition facilitated by reactive solvents such as acetone, nitric acid, ammonia, glycol, water, ethanol, catalytic, benzyl alcohol, or supercritical fluids. To improve recycling efficiency and preserve mechanical properties of the reclaimed fibers, researchers have focused on solvolysis strategies employing diverse solvents[6,9] and catalysts,[10] various temperatures and pressures,[11] processing aids (such as stirring,[12] ultrasounds,[13] and fiber washing[14]), and pretreatment.[15] Solvolysis, recognized for its lower operational temperatures relative to pyrolysis and its capacity to yield fibers with favorable surface and mechanical characteristics, is emerging as a promising recycling method for composite wind turbines.[16–19] Furthermore, chemical recycling, including solvolysis, is among the most widely considered recycling technologies for the next generation of composites to be used or developed for recyclable wind turbine blades.[20]

Solvolysis of composites includes several physical processes, notably flow of solvent, solvent diffusion in polymer matrix, phase transition from solid polymer to solution, and movement of solid/liquid boundary. Computational modeling of solvolysis for composites is important for the optimization of solvolysis techniques as it can provide insight into the depolymerization mechanism and theoretical guidance on the evaluation and

Y. Chen, L. Mishnaevsky Jr.
Department of Wind and Energy Systems
Technical University of Denmark
Roskilde 4000, Denmark
E-mail: yiach@dtu.dk

The ORCID identification number(s) for the author(s) of this article can be found under https://doi.org/10.1002/adem.202302150.

DOI: 10.1002/adem.202302150

optimization of recycling methods. However, the complexity and multitude of interacting processes pose significant challenges, resulting in limited work on modeling.

For the analysis of the epoxy dissolution kinetics via mild alcoholysis, Kuang et al.[21] developed a so-called surface layer model with three layers (gel layer, solid swollen layer, and pure polymer layer). The authors determined the dissolution rate during the diffusion-rate-controlled dissolution process and observed that the solvent with larger diffusivity and better solubility leads to a higher alcohol/catalyst concentration in the gel layer and promote faster dissolution of epoxy. Hammel, Kuang, and Qi[22] developed a reaction–diffusion model for chemical recycling of epoxy resin and composites, involving chemical species concentration-dependent diffusion and reaction rates. They applied the model to multiphase structure and studied the effect of reinforcement on the dissolution process of composites. Yu et al.[23] developed a multiscale modeling framework, with the macroscale mass transportation model and microscale chain diffusion, and used it to analyze the dissolution behavior of covalent adaptable networks. Furthermore, Shi et al.[24] developed a multiscale chemomechanics theory for the dissolution and repolymerization of covalent adaptable network polymers. The theory was based on the statistical analysis of segment length distribution and network degree of curing in the polymers, and a continuum-level model of the thermomechanical properties of polymers at different curing states. The model enabled the prediction of the conversion ratio of functional groups, solution viscosity, volume shrinkage, and glass transition behaviors of repolymerizing networks. Luo et al.[25] developed a multiscale diffusion–reaction computational model, linking the microscale bond exchange kinetics to the continuum-level diffusion and depolymerization in composites. The authors studied the influence of fiber arrangement and other parameters on composite depolymerization.

For the comparative analysis of solvolysis technologies across various polymer scenarios, developing a general, phenomenological model that correlates output parameters (time, energy, quality of recyclate) with input parameters (temperature, physical characteristics) would be advantageous. Furthermore, polymer composites in wind energy deviate significantly from ideal structures, exhibiting numerous defects such as voids, poorly cured regions, and microcracks.[26] Such defects dictate the deformation and damage behavior of these composites throughout their lifecycle and impact the depolymerization process during chemical recycling. Therefore, this article investigates the influence of manufacturing defects on the chemical recycling of composites and explores potential correlations between defects formed during manufacturing and recycling efficiency.

This article aims to provide a computational framework for modeling the solvolysis of composite blades based on a continuum mechanics/micromechanics approach. The dissolution of polymers was described as a phase transition process, analogous to the way fractures or material damages are considered phase transitions from a thermodynamic perspective (refer to 27,28]). Due to their cross-linked chemical structure, thermosets are more challenging for recycling than thermoplastics. Consequently, the model was calibrated and validated using epoxy-based composites materials. The model was applied to examine how imperfections and manufacturing defects within composite structures influence the depolymerization process. The effect of voids, variations in interfiber distances, and poorly cured regions on the depolymerization rate were investigated in numerical experiments. In conclusion, the authors demonstrated that the quality of recycled fibers depends on the distribution of defects within the composites. Therefore, considerations for the postdecommissioning use of composite parts (e.g., fibers) should be integrated into the optimization of composite manufacturing technologies.

2. Computational Micromechanical Model of Dissolution as Phase Transition

2.1. Dissolution as Phase Transition: Phenomenological Model

During solvolysis, the dissolution of the polymer matrix occurs concurrently with the flow and diffusion of the solvent. The dissolution of polymer matrix in solvent is a complex process involving swelling, mass transport, chemical reaction, and phase transition, characterized by two moving fronts indicating polymer dissolution and solvent diffusion.[29,30] **Figure 1** illustrates a schematic of the diffusion–dissolution process. The diffusion and dissolution fronts divide the liquid–solid system into three layers. The dissolution front between the liquid and gel layers distinguishes the dissolved and undissolved polymer. It should be noted that within the gel layer, solvent molecules transition from a free state (liquid) to a hindered state (gel) with the diffusivity decreased. As the chemical reaction progresses and cleavable bonds break, the old dissolution front vanishes along with the dissolved polymer, and a new front forms. The solvent continuously diffuses into the polymer, forming a diffusion front where the solvent concentration reaches a defined value, triggering the chemical reaction. To numerically simulate the phase transition from solid polymer to dissolved polymer, a phenomenological approach was employed. The two phases were characterized by different properties.

The condition of the transition can be defined by a function of temperature and concentration of solvent at a given point. This approach adheres to a modified solid-state reaction law,[31] which describes the rate of polymer dissolving as follows

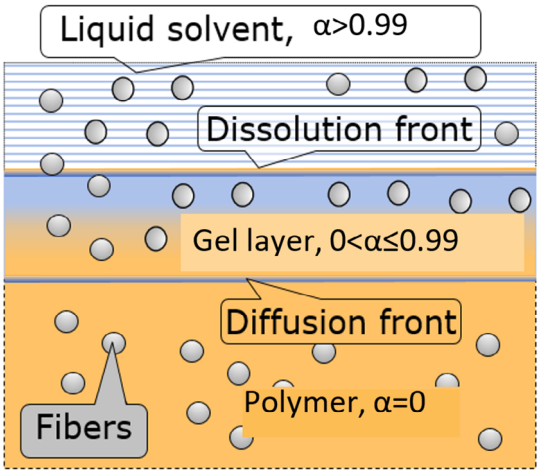

Figure 1. Schema diagram of diffusion–dissolution process.

$$\frac{d\alpha}{dt} = Ag(c)e^{-(E_a/RT)}f(\alpha) \tag{1a}$$

$$g(c) = 1 - \exp(-Bc) \tag{1b}$$

where A is a frequency factor, E_a is the activation energy (kJ mol^{-1}), T is the absolute temperature (K), c is the solvent concentration in the polymer, and R is the universal gas constant (8.31 J mol^{-1} K^{-1}). Due to the interaction between the diffusion and the dissolution process, polymer dissolution can be diffusion-controlled where the diffusion rate is slower than dissolution rate and dissolution-controlled where the dissolution rate is slower. Therefore, a function scaling from 0 to 1 based on solvent concentration in the polymer, $g(c)$, is introduced to the dissolution rate, where B is a constant. $f(\alpha)$ is a function depending on the reaction mechanism, and α is the reacted fraction of polymer at current time t. For polymer dissolving, α can be defined by

$$\alpha = \frac{m_0 - m_t}{m_0} = \frac{m_d}{m_0} \tag{2}$$

where m_0, m_t, and m_d are polymer's initial, current, and dissolved weight, respectively. Ignoring swelling and density change due to solvent diffusion, Equation (2) is rewritten as

$$\alpha = \frac{V_d}{V_0} \tag{3}$$

where V_d and V_0 are polymer's dissolved and initial volume, respectively. For an infinitesimal polymer element, α is used to indicate the dissolution degree, such that the polymer is in solid state when $\alpha = 0$, and it is being dissolved (in the gel layer) when α is approaching 1. In this study, the polymer is declared to be dissolved when $\alpha > 0.99$.

The reaction function $f(\alpha)$ is described by a 3D diffusional model.[31] The model is commonly used to describe the reaction between a diffusing and a solid reactant where a product layer formed during the process can be regarded as the gel layer

$$f(\alpha) = \frac{3(1-\alpha)^{2/3}}{2[1-(1-\alpha)^{1/3}]} \tag{4}$$

Combining Equation (1) and (4) gives a reacted fraction in the discrete form as

$$\begin{aligned}\alpha_{n+1} &= \alpha_n + Ag(c)e^{-\left(\frac{E_a}{RT}\right)}f(\alpha)\Delta t \\ &= \alpha_n + A(1-e^{-Bc})e^{-(E_a/RT)}\frac{3(1-\alpha)^{2/3}}{2[1-(1-\alpha)^{1/3}]}\end{aligned} \tag{5}$$

2.2. Solvent Transport and Diffusion

The balance of the solvent transport can be written in a partial differential form[32] as

$$\frac{\partial c}{\partial t} = -\nabla J + H \tag{6}$$

where H is the volumetric change rate of solvent concentration due to polymer dissolution and J is the flux of the solvent.

The solvent transport into the polymer is described by Fick's law as

$$J = -D\nabla c \tag{7}$$

where D is the diffusivity of solvent transport into the polymer. Substituting Equation (7) into (6) yields

$$\frac{\partial c}{\partial t} = -D\nabla^2 c + H \tag{8}$$

As Figure 1 shows, the diffusivity remains at a low level in the solid layer and increases in the gel layer due to the degradation of polymer matrix. Some experiments have shown that the solvent diffusivity during polymer dissolution depends on reaction environment and progress, such as temperature, cross-link density,[6,33] and solvent concentration.[34] Thus, the diffusivity is described by a function of both temperature and dissolution degree in exponential fashion[35,36]

$$D = D_0 e^{\frac{-E_a}{RT}} e^{\beta\alpha^2} \tag{9}$$

where β is a parameter constant and D_0 is a reference diffusivity.

The swelling due to solvent uptake, and thus the change of polymer density, is not considered. Considering an infinitesimal polymer cube, as the material is dissolved, the space is occupied by the same volume of solvent. Assuming the solvent concentration in the whole system remains the same, the solvent concentration of this cube can be described as

$$c = c_0\alpha \tag{10}$$

where c_0 is the constant solvent concentration in the system. Submitting Equation (10) into (8) obtains

$$H = \frac{\partial c}{\partial t} + D\nabla^2 c = c_0\frac{\partial \alpha}{\partial t} + D\nabla^2 c \tag{11}$$

Ignoring the second-order differential and taking Equation (1) and (4) into account, H is rewritten as

$$H = \frac{3}{2}\gamma c_0(1-e^{-Bc})e^{-(E_a/RT)}\frac{(1-\alpha)^{2/3}}{1-(1-\alpha)^{1/3}} \tag{12}$$

where γ is an adjustment factor determined by the dissolution experiment.

The model was implemented in the commercial finite element software package Abaqus 2022. Due to the analogy between heat and mass transfer, the diffusion of solvent is simulated using a heat transfer analysis. The finite element approach for the diffusion–dissolution process is presented in **Figure 2**. For each element, the chemical reaction begins when the solvent concentration c reaches a defined value c_r. At the beginning of each time increment Δt, the increase of reacted fraction $\Delta\alpha$ is calculated if the chemical reaction has started and the element is not dissolved ($\alpha \leq 0.99$). Otherwise, the reacted fraction increment equals to 0. The reacted fraction α is consequently updated and used to determine the diffusivity of solvent into the polymer, D, via the user subroutine user-defined field (USDFLD). When the chemical reaction is activated, the rate of change of solvent concentration due to polymer dissolution, H, is obtained using the user

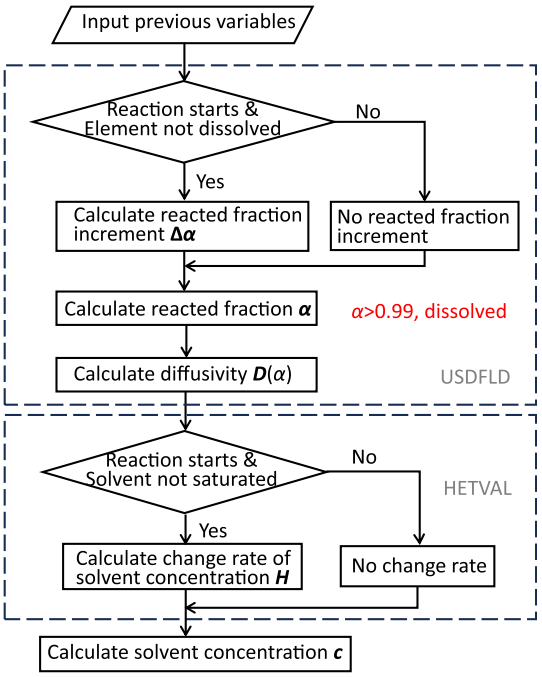

Figure 2. Implemented finite element approach for diffusion–dissolution process at current time increment.

subroutine heat flux (HETVAL). In the end of the time increment, the solvent concentration c was subsequently updated by D and H.

2.3. Defects in Blade Composites and Their Potential Influence

As noted above, wind blade composites can contain a rather high amount of defects, formed during manufacturing.[26] In this work, it is assumed that these defects might influence both the service behavior of blades (e.g., damage and failure likelihood, necessity for maintenance) and the recycling process.

The manufacturing of composite blade structures is typically based on a vacuum infusion process, during which a liquid resin flows into the dry fibrous reinforcement materials, as shown in **Figure 3**, before curing to form the final composite material. Due to the scale and complexity of the different material systems in the blades, ensuring proper infiltration of resin between fibers, managing thermal gradients, and achieving uniformity of curing throughout the blade face significant challenges. This process can produce considerable porosity and voids or result in significant heterogeneity in the degree of cure throughout the structure. Both scenarios can adversely affect the quality of the final products. Regions that are improperly cured and voids formed during manufacturing constitute potential defect areas in composites when subjected to mechanical impact or cyclic loading. Furthermore, poorly cured regions exhibit different diffusion coefficients, influencing moisture uptake in the composite and potentially reducing the composite's lifetime.

In addition to triggering damage initiation and causing the early failure of in-service blades, poorly cured and porous regions within composites also influence the composite recycling process. The solvolysis of composites, controlled by diffusion and reaction processes, is influenced by both the nano- and microscale porosity, as well as the diffusion coefficient within the polymer regions.

Assuming that the postcuring porosity includes only nanoscale to very small voids, much less than fiber diameters or interfiber distances, one considers here the diffusion coefficient as influenced by low-scale porosity. In this case, the equivalent diffusion coefficient is determined by using the coefficient

$$D_{\mathrm{d}} \approx \psi D \tag{13}$$

where ψ is defined as a constant of 0.707 or the product of 0.66 and porosity.[37] In refs. [38,39], the diffusion coefficient is

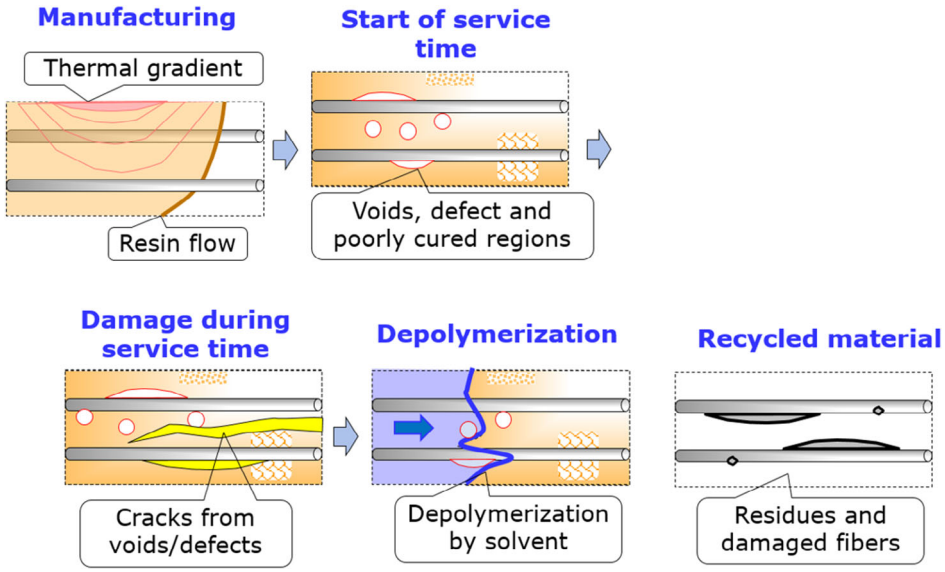

Figure 3. Schema of the influence of manufacturing defects (poorly cured regions, voids, microcracks) on the lifetime of blades, recycling, and quality of recyclate.

determined as an increasing function of the degree of polymerization. Therefore, it is further assumed that the polymer's diffusion coefficient changes depending on the degree of polymerization and porosity of the composite regions.

Furthermore, variations in the nanoscale properties of polymers manifest in the vicinity of polymer/fiber interface.[40] Compositional gradients near the fiber/matrix interfaces were observed, causing property differences between the interphase region and the bulk matrix, including a lower interphase glass transition temperature, T_g. According to ref. [39], a lower glass transition temperature near the interfaces is associated with a higher diffusion coefficient in these regions.

The heterogeneity of the polymer matrix would supposedly influence the process of depolymerization of composites during solvolysis, potentially contributing to the presence of residues on the surfaces of recycled fibers. The fibers with adherend residues generally have less value for postrecycling utilization as additional washing steps are required.[41] Therefore, this study concentrates on exploring the effects of variations in the diffusion coefficient, fiber arrangement, and presence of voids on the solvolysis process of composites.

2.4. Determination of Model Parameters and Validation

It should be noted that this work focuses on the computational modeling of solvolysis of composites without experimental investigations. To illustrate the procedure for determining the modeling parameters, this research utilized the results from dissolution tests on an anhydride-cured thermosetting epoxy, as conducted by Luo et al.[25] Block samples with squared cross-sectional dimensions of 11 mm × 11 mm and length of 65 mm were immersed in ethylene glycol (EG) mixed with the catalyst triazabicyclodecene at 140 °C. They were removed from the solution to dry before weighing at specific time intervals. The details of the test can be found elsewhere.[25]

Due to the large ratio of the sample length to the cross-sectional dimension (65 mm/11 mm), a 2D plane strain analysis was considered. Under the guidance of a convergence study, the cross-sectional model was meshed with 8464 4-node linear quadrilateral elements. The bottom surface was constrained in all degrees of freedom while an initial temperature representing the initial solvent concentration c_0 (2.2×10^{-6} mol m^{-3}) was mapped to four sides of the model for free diffusion.

Luo's team presented diffusivity as a function of temperature and depolymerization degree (similar to the reacted fraction α). Given the same material and experimental conditions, the parameters of diffusivity (D_0 and β in Equation (9)) were determined by comparing to the mean value of the diffusivity obtained by Luo et al. The parameter B from the scaling function (Equation (12)) was determined by the concerns that $g(c)$ should approach 1 at the initial concentration. The constants A and γ from Equation (1) and (12), which are related to the polymer reaction rate, were obtained by fitting the polymer dissolution test, as shown in **Figure 4**. The model shows favorable agreement with experiment for the first 180 min where the cross section shrinks along four edges with the solvent getting into the epoxy. As time increases, the simulated sample results in a smaller and rounder shape, potentially attributable to the absence of swelling effect and the excessive evolution of solvent concentration at the corners. Modifications are necessary for future study. Given the overall favorable agreement with experimental results, the model is used for this work. The model parameters are listed in **Table 1**.

3. Parametric Studies

3.1. Effect of Variability of Diffusion Coefficients on the Dissolution Process

As discussed in Section 2.3, porosity near the polymer/fiber interface can result in varying diffusivities. To investigate the influence of diffusivity on the dissolution process, a square 2D unit cell model with a side length of 0.015 mm, as shown in **Figure 5**a, was considered as shown in Figure 5a. The diameter of each fiber is 7 μm. The interface layer model proposed in ref. [42] was used to account for the role and impact of sizing and the fiber/matrix interface in the composites. The thin layers surrounding fibers include sizing and interface regions, reflecting the peculiar properties of these interface regions. The thickness of the surrounding layers is one-tenth of the fiber diameter. It is assumed that these layers can contain interface defects, exhibiting varied diffusivity. The diffusivity ratio of this interface region to the matrix area, denoted as D_i/D_m, was varied as 0.1, 0.5, 1, and 1.5.

The dissolution times required for the complete dissolution of the matrix in the unit cell models were determined by the computational simulation. The normalized dissolution times for each diffusivity ratio are listed in **Table 2**. As expected, increased diffusivity within the interface area leads to accelerated dissolution. Given that the model exhibited comparable dissolution behaviors

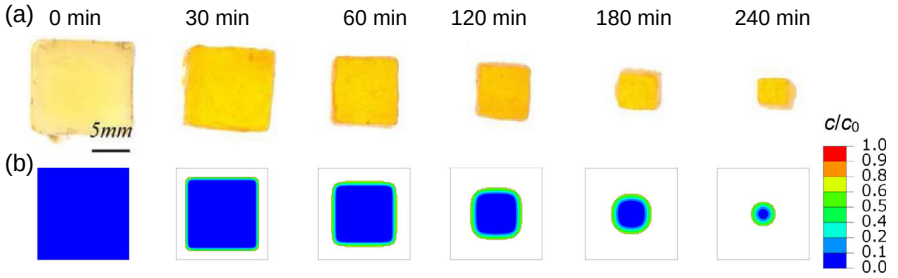

Figure 4. Dissolution of epoxy sample over time from a) experimental testing (reprinted with permission,[25] Elsevier) and b) numerical modeling. The contour refers to the solvent concentration normalized by the initial solvent concentration (c/c_0). Details of the experiment can be found elsewhere.[25]

Table 1. Model parameters.

Parameter	Description	Value	Unit
D_0	The reference diffusivity	4.1×10^7	$mm^2\ s^{-1}$
β	A constant for diffusivity	2.8	–
E_a	The activation energy	93	$kJ\ mol^{-1}$
B	A constant for the rate of dissolution	1.6×10^6	$m^3\ mol^{-1}$
c_0	The constant solvent concentration in the system	2.2×10^{-6}	$mol\ m^{-3}$
A	A frequency factor	5.87×10^{10}	–
γ	An adjustment factor for the change of solvent concentration due to dissolution	5.4×10^7	–

for diffusivity ratios of 0.5, 1, and 1.5, only the simulated processes corresponding to the ratios of 0.1 and 1 are compared in Figure 5b,c. A decrease in diffusivity at the interface region ($D_i/D_m = 0.1$) results in slower solvent diffusion across the entire cell and a significantly retarded diffusion around the fibers. Consequently, the matrix surrounding the fibers disappears later than the matrix between the fibers, contrasting with observations at other diffusivities, including $D_i/D_m = 0.5$.

Table 2. Normalized dissolution time at varying diffusivity ratios.

D_i/D_m	0.1	0.5	1	1.5
Normalized dissolution time	1.32	1.14	1	0.90

3.2. Effect of Diffusion and Reaction Rates

Polymer dissolution arises from the combined contributions of diffusion and reaction processes. To study the effects of reaction and diffusion rates, as well as their coupling effect, on composite dissolution, a parametric study was performed using the previously mentioned unit cell model with $D_i/D_m = 1$, and the results are presented in Figure 7. The studied parameters, namely, the diffusivity D_m and the parameter A associated with reaction rate, were normalized with respect to the parameters utilized in the modeling described in Section 3.1. Furthermore, the simulated dissolution times were normalized against the corresponding result in Figure 5c. The normalized diffusivity D_m varied from 0.2 to 2, and the normalized reaction parameter A varied from 1 to 20.

From **Figure 6**, increasing both the diffusivity and reaction parameter brings out the fastest dissolution, whereas reducing

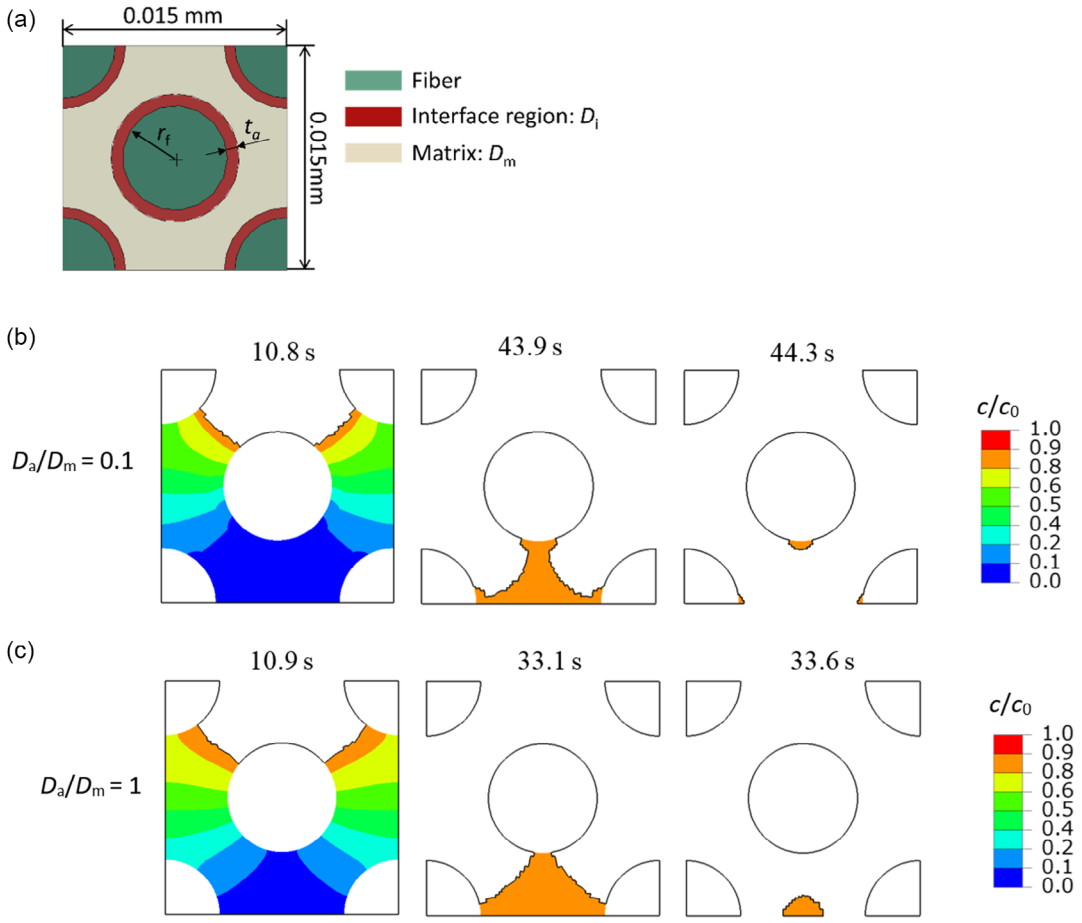

Figure 5. Sketch geometry of a) a unit cell with an area adjacent to the fibers, and simulated dissolution processes with the diffusivity ratio, D_a/D_m, of b) 0.1 and c) 1. The contour refers to the normalized solvent concentration c/c_0.

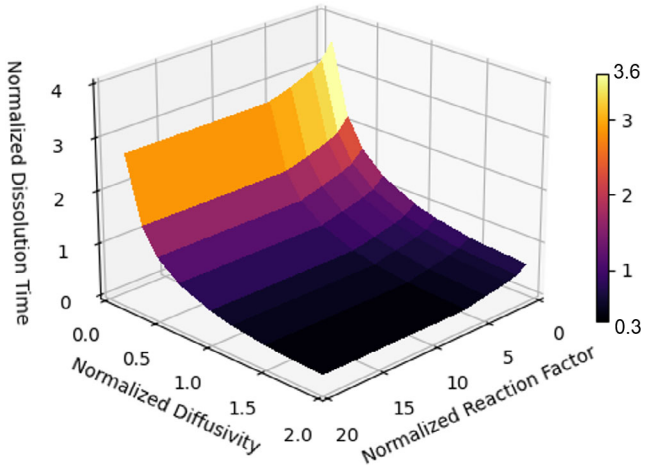

Figure 6. Simulated dissolution time of a unit cell with varying diffusivities and reaction rates. Each dissolution time is normalized to the model in Figure 5c.

both parameters yields the opposite result. Compared to the reaction parameter, varying the diffusivity leads to a more pronounced effect on the dissolution time. Therefore, it can be inferred that the dissolution process is dominated by diffusion. For instance, at a low reaction factor ($A = 1$), increasing the diffusivity leads to an 82% reduction in dissolution time. This effect arises from the fact that higher diffusivity speeds up solvent transport into the polymer, thereby advancing the onset of the chemical reaction. However, at a low diffusivity ($D_m = 0.2$), an increase in the reaction parameter only diminishes the dissolution time by 21%, attributable to the sluggish movement of the diffusion front hindering the reaction.

Similar trends have been observed in experimental studies. Ma and Mutt[43] found that the slow diffusion of solvent within a highly cross-linked matrix significantly limited the recycling rate of composites through acid digestion, even in the presence of a rapid reaction rate. Vallee et al.[44] investigated the solvolysis of sheet-molding composites using a paste consisting of an unsaturated polyester–styrene resin. They observed that the dissolution was initially governed by reaction kinetics at the sample's surface, transitioning to diffusion controlled as the solvent and degradation products permeated the polymer. Therefore, the parametric study implies that enhancing the solvent diffusivity into the polymer, achievable by shredding or pretreatment, constitutes a more effective strategy for accelerating solvolysis than merely speeding up the reaction rate.

3.3. Effect of Fiber Arrangement

In composites, fibers are often arranged in a nonideal or random manner, with regions of high fiber density constituting some of the most common defects of composites. The impact of fiber density variation on the depolymerization process was examined using a square model measuring 0.08 mm by 0.08 mm. Fibers with a diameter of 7 μm are randomly distributed within the model, with volume fractions varying from 20% to 60%. **Figure 7** displays the predicted dissolution appearance at the tenth minute and the dissolution times corresponding to each fiber volume fraction. It can be seen from Figure 7f that the dissolution time increases at a faster rate as the fiber volume fraction becomes larger. Fibers act as barriers to solvent diffusion.[45] With a higher

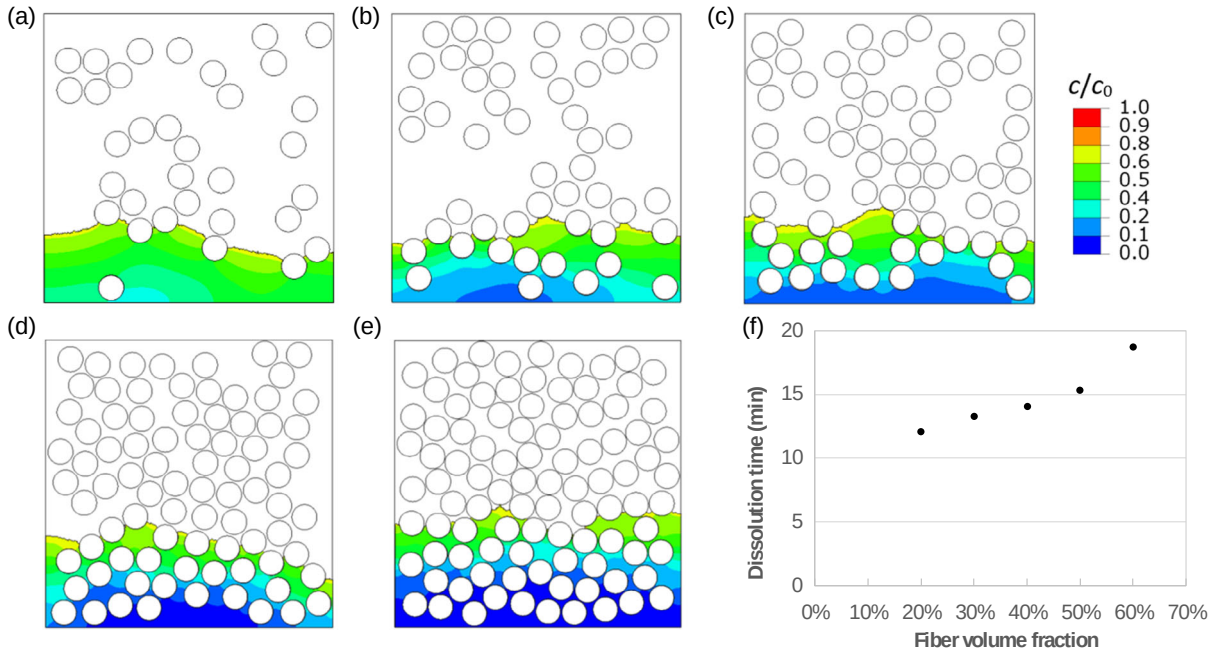

Figure 7. Predicted appearance of a square composite sample with fiber volume fraction of a) 20%, b) 30%, c) 40%, d) 50%, and e) 60% at the tenth minute during the dissolution process, and f) the predicted dissolution time as a function of fiber volume fraction. The contour refers to the normalized solvent concentration c/c_0.

concentration of fibers, solvent molecules have to navigate a more tortuous path to permeate the matrix, elongating the pathway and slowing down the diffusion process. As the solvent diffusion process is integral to the dissolution of the matrix, access to the reactive site is also hindered by higher fiber fractions, affecting the reaction rate. Therefore, a more homogeneous distribution of fibers is expected to ensure more homogeneous depolymerization and better quality of recyclates.

3.4. Influence of Voids and Dry Spaces

Voids and dry regions are common defects in blade composites, especially when fibers are located closely, and resins cannot penetrate this region or air bubbles are trapped in the resin during manufacturing. It is of interest to investigate how the pores and voids influence the depolymerization process.

A square model measuring 0.08 mm by 0.08 mm is depicted in **Figure 8**. The fibers, uniformly distributed, possess a diameter of 7 μm and comprise a volume fraction of 40%. Diffusion is assumed to initiate from the top surface. Contrary to fibers, voids become filled with solvent immediately upon the penetration or influx of solvent molecules. Therefore, three semicircles located on the top surface were used to represent the voids, with an initial solvent concentration applied to the surfaces of these voids as they become filled with solvent. The dissolution time for the model, with and without the presence of voids, is 806 and 810 s, respectively. Upon examining Figure 7b, an increase in dissolution is observed from the right to the left side in the model featuring voids, aligning with the absence of voids on the right side of the top surface.

A unit cell with a length of 10 μm was used to examine how voids accelerate the dissolution process, as depicted in **Figure 9**. In the model considering solvent diffusion on the void (Figure 9b), both the top and void's surfaces were treated as a solvent–polymer interface with a boundary condition of solvent concentration (represented by rectangles). However, in the model without diffusion on the void (Figure 9c), only the top surface was subjected to the solvent concentration. The diameter of fiber is 7 μm and the ratio of the void radius to fiber radios (r_v/r_f) varied from 0 to 0.35. The reduction of dissolution time, t_r, is defined as

$$t_r = \frac{t_t - t_v}{t_t} \times 100\% \tag{14}$$

where t_t and t_v are the dissolution time of the cell without (Figure 9c) and with (Figure 9b) void diffusion, respectively. **Figure 10** plots the reduction of dissolution time as a function of radius ratios. It is observed that the greater the void in the model, the more rapid the polymer dissolution. This phenomenon can be explained by comparing the simulated appearances of unit cells during the dissolution process, as shown in **Figure 11**. The void increases the solvent contact area and broadens the diffusion path (Figure 11a), contributing to the accelerated dissolution. In addition, the effect of voids becomes negligible as the ratio of void radius to fiber radius is less than 0.05.

3.5. Model Validation

Using the calibrated parameters above, the model was compared with Luo's model[25] in predicting the dissolution process of a

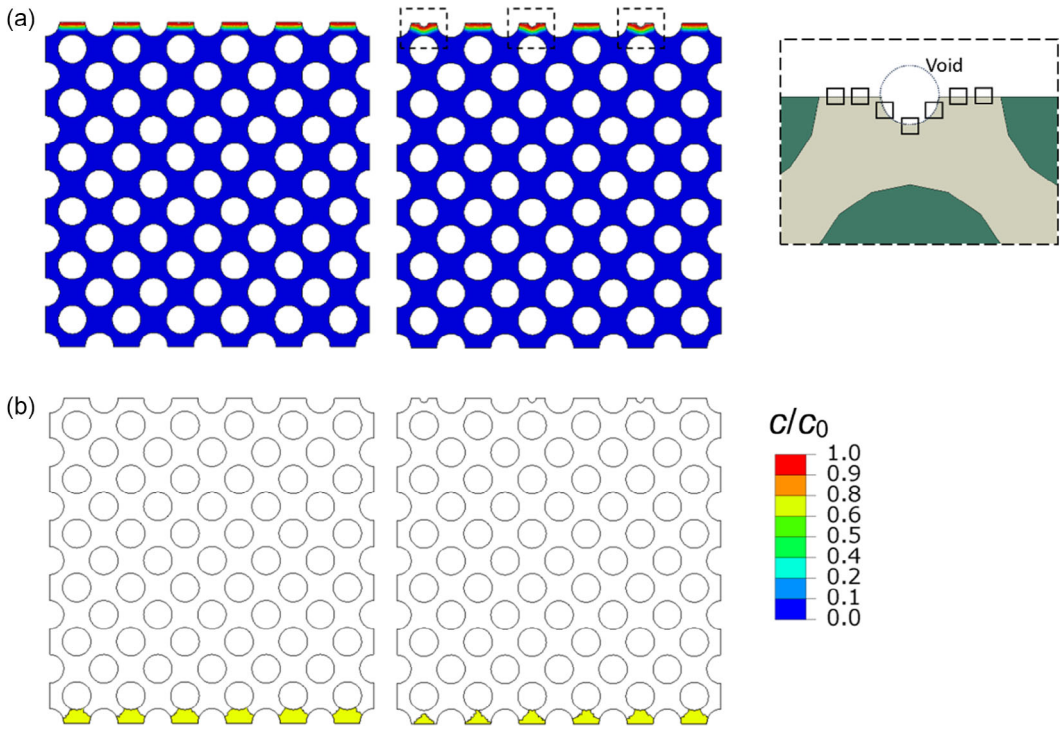

Figure 8. The comparison of simulated depolymerization for a composite model considering the effect of voids at a) the beginning and b) end of the process. The contour refers to the normalized solvent concentration.

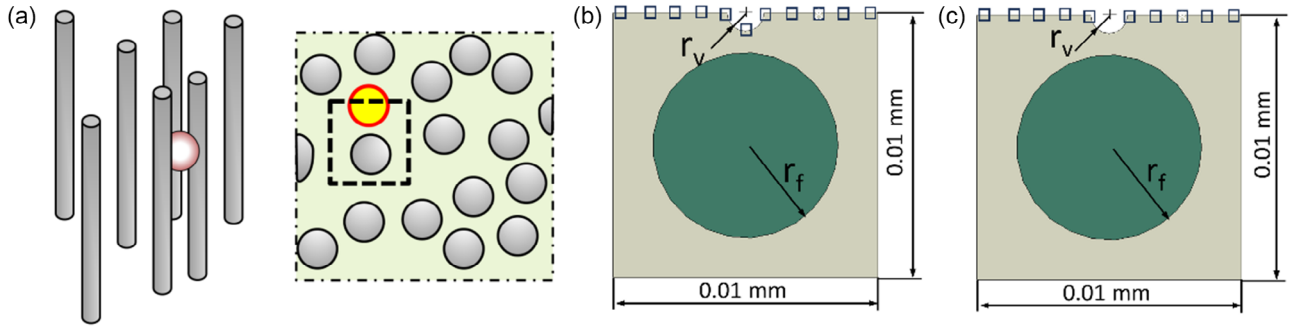

Figure 9. Sketch geometry of a) voids in composites and the unit cells designed for the analysis with an initial solvent concentration (represented by rectangles) on b) the top and void's surface and c) the top surface only.

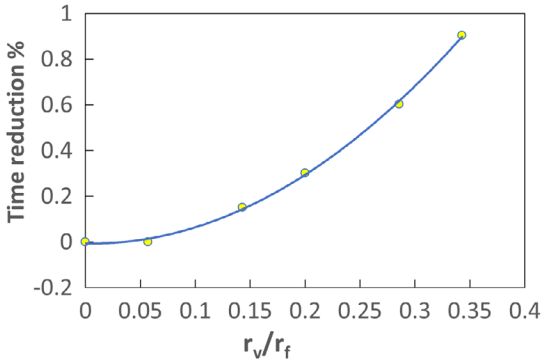

Figure 10. Reduction of dissolution time as a function of the void-to-fiber radius ratio.

composite sample, as shown in **Figure 12**. The dimensions of the cross section are 0.08 mm × 0.08 mm, with the fiber volume content of 40%. The diameter of each fiber is 7 μm. The diffusion and depolymerization started from the top surface where the boundary condition was defined by an initial solvent concentration. As the area of initial diffusion has changed from a pure polymer sample ($11 \times 65\ mm^2$) to a composite sample ($0.08 \times 100\ mm^2$), the reference diffusivity D_0 in Table 1 was divided by a ratio of these two areas (89) for parameter adjustments.

The dissolution front moves with time and the proposed model shows dissolution rates comparable to Luo's model. It can be seen from the proposed model that the diffusion front moves deeper into the epoxy area as time progresses, while Luo's model showed no significant diffusion. The variance is attributed

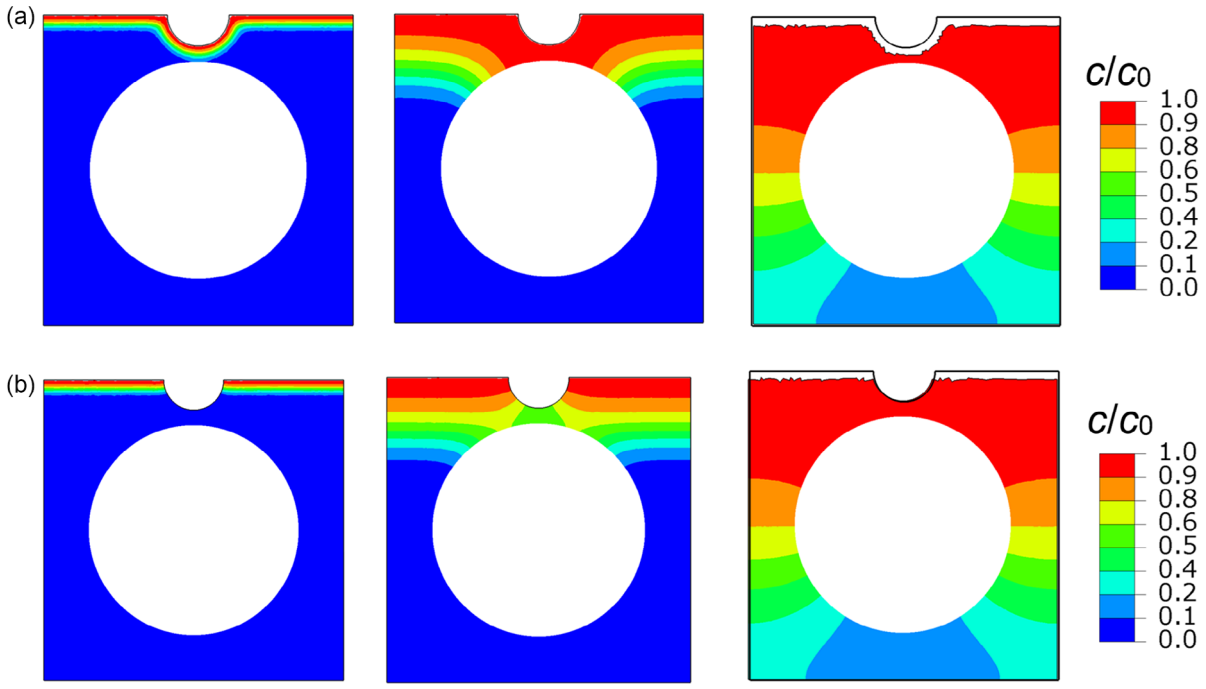

Figure 11. Comparison of simulated dissolution process of a unit cell with $r_v/r_f = 0.29$. An initial solvent concentration is provided on a) the top and void's surfaces and b) the top surface only. The contour refers to the normalized solvent concentration.

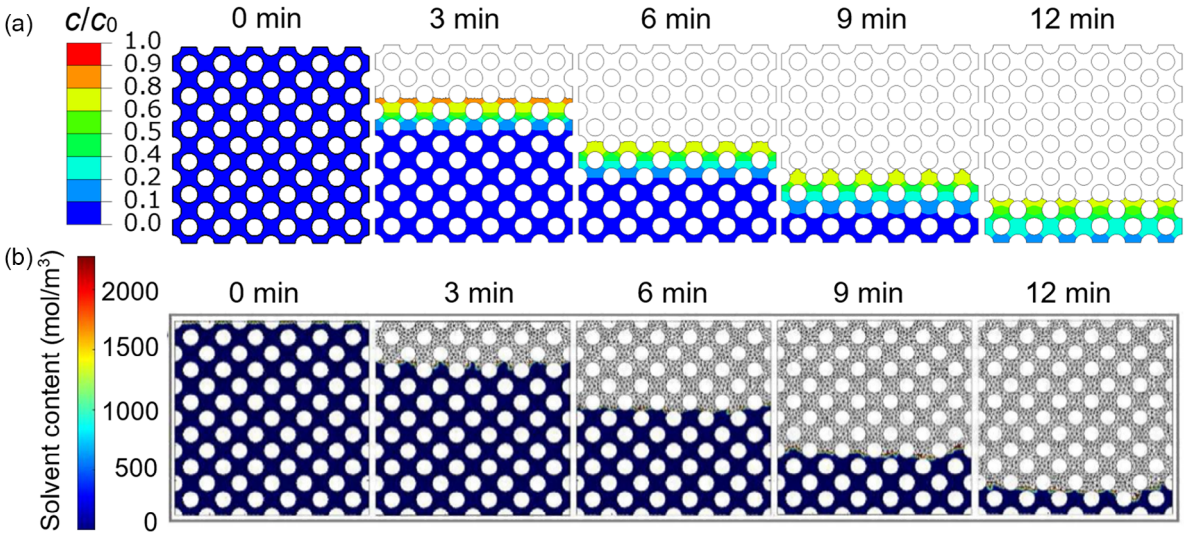

Figure 12. The simulated depolymerization of an epoxy matrix composite material with 40% carbon fiber by a) the proposed model and b) Luo's model (reprinted with permission.[25] Elsevier). Details of Luo's model can be found elsewhere.[25]

to the different approaches applied to the reacted fractions. The proposed model allowed the reacted fraction to increase gradually with rising solvent concentration, facilitating solvent diffusion before the element totally dissolved. Luo's model suggested an instant increase of the reacted fraction at the liquid–solid interface to constrain solvent diffusion.

4. Conclusions

A computational model of depolymerization of composites during the solvolysis for wind turbine blades was developed. The model is based on a phenomenological approach describing the dissolution of epoxy matrix by a local phase transition with considerations of temperature, solvent diffusion, and local microstructures. This has been implemented in Abaqus with the user subroutines of USDFLD and HETVAL. The calibration of the model from experimental data (the diffusion test for a thermosetting epoxy immersed in EG at 140 °C and corresponding dissolution test with catalyst) is demonstrated. The model has been validated against literature data.

Parametric studies were conducted to assess the effect of defects and material heterogeneity on depolymerization. It was demonstrated that voids in the polymer lead to local acceleration of the polymer dissolution. Fiber volume fractions and distributions show coupling effect on the dissolution rates of polymers. The solvent diffusion between closely located fibers evolves more slowly and results in slower dissolution. Further, variation of the diffusion coefficient in the composite matrix leads to nonhomogeneity of depolymerization and may explain remaining residues on the fibers. The conclusion is that the homogeneity and quality of recycled fibers depends on the manufacturing quality of composites, while voids, variations of fibers density, and inadequately cured regions lead to variations in the depolymerization rate and thus to residues on fibers, and lower quality recyclates.

Acknowledgements

The authors acknowledge the financial support of the Innovation Foundation of Denmark in the framework of project "WiseWind: New generation of sustainable wind turbine blades" (http://wisewind.dtu.dk/), grant no. 2079-00004B. L.M. is grateful to the support of the European Commission via Horizon project "Blades2Build: Recycle, repurpose and reuse end-of-life wind blades composites: A coupled pre- and co-processing demonstration plant," grant no. 101096437, and of the Ministry of Foreign Affairs of Denmark via Danida grant no. 19-M02-DTU "Maintenance and repair strategy for wind energy development" (http://maintainergy.dk).

Conflict of Interest

The authors declare no conflict of interest.

Data Availability Statement

The data that support the findings of this study are available from the corresponding author upon reasonable request.

Keywords

recyclable composites, solvolysis, sustainability, wind energy

Received: December 14, 2023
Revised: March 21, 2024
Published online: May 2, 2024

[1] W. Europe, *The European Wind Industry's Views on Managing Wind Energy Assets at The End of their Operational Lifetime*, Wind EUROPE, Brussels, Belgium **2017**.
[2] M. Ierides, J. Reiland, A. Dierckx, *Wind Turbine Blade Circularity: Technologies and Practices Around The Value Chain*, Bax and Company, Barcelona, Spain **2019**.

[3] C. Martin, Wind Turbine Blades Can't Be Recycled, So They're Piling Up in Landfills, https://www.bloomberg.com/news/features/2020-02-05 (accessed: February 2020).
[4] Working Towards a European Standard for Decommissioning Wind Turbines, https://windeurope.org/newsroom/news/working-towar (accessed: July 2020).
[5] Wind Turbines are Getting Old. What happens to the Ageing Fleet?, https://www.france24.com/en/tv-shows/down-to-earth (accessed: January 2023).
[6] C. Mattsson, A. André, M. Juntikka, T. Tr nkle, R. Sott, *IOP Conf. Ser. Mater. Sci. Eng.* **2020**, *942*, 012013.
[7] M. J. Leon, *Curr. Opin. Green Sustainable Chem.* **2023**, *39*, 100746.
[8] Y. Yang, R. Boom, B. Irion, DJ van Heerden, P. Kuiper, H. de, *Chem. Eng. Process: Process Intensif.* **2012**, *51*, 53.
[9] C. Tschentscher, M. Gebhardt, S. Chakraborty, D. Meiners, in *Proc. of the Symp. Materialtechnik, Clausthal-Zellerfeld, Germany* **2021**, pp. 25–26.
[10] R. Muzyka, S. Sobek, A. Korytkowska-Wałach, Ł. Drewniak, M. Sajdak, *Sci. Rep.* **2023**, *13*, 9270.
[11] R. Piñero-Hernanz, C. Dodds, J. Hyde, J. Garcia-Serna, M. Poliakoff, E. Lester, M. J. Cocero, S. Kingman, S. Pickering, K. H. Wong, *Compos. Part A: Appl. Sci. Manuf.* **2008**, *39*, 454.
[12] M. Grilc, B. Likozar, J. Levec, *Catal. Today* **2015**, *256*, 302.
[13] I. Meyer zu Reckendorf, A. Sahki, D. Perrin, C. Lacoste, A. Bergeret, A. Ohayon, K. Morand, *Polymers* **2022**, *14*, 1083.
[14] M. J. Keith, G. Oliveux, G. A. Leeke, in *ECCM 2016 - Proceeding of the 17th European Conf. on Composite Materials, Munich, Germany* **2016**, pp. 26–30.
[15] B. Rijo, A. P. S. Dias, J. P. S. Carvalho, *Sustainable Mater. Technol.* **2023**, *35*, e00545.
[16] Reprocessable, Repairable and Recyclable Epoxy Resins for Composites, https://www.compositesworld.com/articles/reprocessable-repairable-and-recyclable-epoxy-resins-for-composites (accessed: May 2021)
[17] A.-C. Johansson, R. Sott, C. Mattsson, in Comparative Study of Thermochemical Recycling with Solvolysis and Pyrolysis of End-of-Life Wind Turbine Blades: Rekovind2-WP3, https://wwww.diva-portal.org/smash/get/diva2:1780227/FULLTEXT01.pdf.
[18] Vestas Hails Breakthrough for Recyclable Wind Turbines, https://www.energymonitor.ai/renewables/vestas-hails-breakthrough-for-recycling-wind-turbine-blades/?cf-view (accessed: February 2023).
[19] Swancor Launched Recyclable Thermosetting Epoxy Resin "EzCiclo", Leading to Zero-Carbon Era, http://www.swancor.com.cn/en/news_detail.aspx?id=226#:~:text=%22EzCiclo%22%20%26%22%20CleaVER%22&text=Swancor's%20latest%20developmentDegraded%20via%20%22CleaVER%22%20technology.C%20%22EzCiclo%22 (accessed: April 2022).
[20] L. Mishnaevsky Jr., *Energies* **2023**, *16*, 7694.
[21] X. Kuang, Q. Shi, Y. Zhou, Z. Zhao, T. Wang, H. J. Qi, *RSC Adv.* **2018**, *8*, 1493.
[22] C. M. Hamel, X. Kuang, H. J. Qi, *Compos. Part B: Eng.* **2020**, *200*, 108363.
[23] K. Yu, H. Yang, B. H. Dao, Q. Shi, C. M. Yakacki, *J. Mech. Phys. Solids* **2017**, *109*, 78.
[24] X. Shi, D. Soule, Y. Mao, C. Yakacki, H. Lu, K. Yu, *J. Mech. Phys. Solids* **2020**, *138*, 103918.
[25] C. Luo, C. Chung, K. Yu, *Mater. Today Sustainability* **2023**, *23*, 100452.
[26] L. Mishnaevsky, *Materials* **2022**, *15*, 2959.
[27] D. Krajcinovic, A. Rinaldi, *J. Appl. Mech.* **2005**, *72*, 76.
[28] T. Yokobori, *Strength, Fract. Comp.* **2011**, *7*, 1.
[29] B. A. Miller-Chou, J. L. Koenig, *Macromolecules* **2002**, *35*, 440.
[30] N. A. Peppas, J. C. Wu, E. D. von Meerwall, *Macromolecules* **1994**, *27*, 5626.
[31] A. Khawam, D. R. Flanagan, *J. Phys. Chem. B* **2006**, *110*, 17315.
[32] R. B. Bird, W. E. Stewart, E. N. Lightfoot, in *Transport Phenomena*, 2nd ed., John Wiely & Sons, Inc., Hoboken, NJ **2001**.
[33] C. M. Hamel, X. Kuang, K. Chen, H. J. Qi, *Macromolecules* **2019**, *52*, 3636.
[34] J. El Yagoubi, G. Lubineau, A. Traidia, J. Verdu, *Compos. Part A: Appl. Sci. Manuf.* **2015**, *68*, 184.
[35] D. S. Clague, R. J. Phillips, *Phys. Fluids* **1996**, *8*, 1720.
[36] K. J. Laidler, *J. Chem. Educ.* **1984**, *61*, 494.
[37] A. Kantzas, J. Bryan, S. Taheri, Fundamentals of Fluid Flow in Porous Media, https://perminc.com/resources/fundamentals-of-fluid-flow-in-porous-media/ (accessed: June, 2018).
[38] M. C. Griffiths, J. Strauch, M. J. Monteiro, R. G. Gilbert, *Macromolecules* **1998**, *31*, 7835.
[39] O. J. Karlsson, J. M. Stubbs, L. E. Karlsson, D. C. Sundberg, *Polymer* **2001**, *42*, 4915.
[40] M. R. Vanlandingham, R. R. Dagastine, R. F. Eduljee, R. L. McCullough, J. W. Gillespie, *Compos. Part A: Appl. Sci. Manuf.* **1999**, *30*, 75.
[41] G. Oliveux, J. L. Bailleul, E. L. G. La Salle, *Compos. Part A: Appl. Sci. Manuf.* **2012**, *43*, 1809.
[42] L. Mishnaevsky Jr, P. Brøndsted, *Comput. Mater. Sci.* **2009**, *44*, 1351.
[43] Y. Ma, S. Nutt, *Polym. Degrad. Stab.* **2018**, *153*, 307.
[44] M. Vallee, G. Tersac, N. Destais-Orvoen, G. Durand, *Ind. Eng. Chem. Res.* **2004**, *43*, 6317.
[45] S. T. Mileiko, in *Metal and Ceramic Based Composites*, vol. *12*, (Eds: S. T. B. T.-C. M. S. Mileiko), Elsevier, Amsterdam **1997**, pp. 441–474.